Linear Power Spectra in Cold+Hot Dark Matter Models: Analytical Approximations and Applications

Chung-Pei Ma[1]
Theoretical Astrophysics 130-33, California Institute of Technology, Pasadena, CA 91125

ABSTRACT

This paper presents simple analytic approximations to the linear power spectra, linear growth rates, and rms mass fluctuations for both components in a family of cold+hot dark matter (CDM+HDM) models that are of current cosmological interest. The formulas are valid for a wide range of wavenumber, neutrino fraction, redshift, and Hubble constant: $k \lesssim 10\,h$ Mpc^{-1}, $0.05 \lesssim \Omega_\nu \lesssim 0.3$, $0 \leq z \lesssim 15$, and $0.5 \lesssim h \lesssim 0.8$. A new, redshift-dependent shape parameter $\Gamma_\nu = a^{1/2}\Omega_\nu h^2$ is introduced to simplify the multi-dimensional parameter space and to characterize the effect of massive neutrinos on the power spectrum. The physical origin of Γ_ν lies in the neutrino free-streaming process, and the analytic approximations can be simplified to depend only on this variable and Ω_ν. Linear calculations with these power spectra as input are performed to compare the predictions of $\Omega_\nu \lesssim 0.3$ models with observational constraints from the reconstructed linear power spectrum and cluster abundance. The usual assumption of an exact scale-invariant primordial power spectrum is relaxed to allow a spectral index of $0.8 \lesssim n \leq 1$. It is found that a slight tilt of $n = 0.9$ (no tensor mode) or $n = 0.95$ (with tensor mode) in $\Omega_\nu \sim 0.1 - 0.2$ CDM+HDM models gives a power spectrum similar to that of an open CDM model with a shape parameter $\Gamma = 0.25$, providing good agreement with the power spectrum reconstructed by Peacock and Dodds (1994) and the observed cluster abundance.

Subject headings: cosmology : theory – dark matter – elementary particles – large-scale structure of universe

1. Introduction

The linear power spectrum of a given cosmological model serves as the basic input for most linear calculations of large-scale structure and numerical simulations of gravitational collapse. The computation of the power spectrum involves numerical integration of the linearized, coupled Einstein, Boltzmann and fluid equations that govern the evolution of the metric perturbations and

[1]e-mail: cpma@tapir.caltech.edu

the density fields of different particle species. The calculations become increasingly complicated as more particle species are included, with those for massive neutrinos being the most time-consuming due to their time-dependent energy-momentum relation and nonzero anisotropic stress (Ma & Bertschinger 1995 and references therein).

The Boltzmann integration is necessary for obtaining highly accurate power spectra, but when an accuracy of $\lesssim 10\%$ is all that is desired, analytic approximations can be very useful and illuminating. The power spectra for $\Omega = 1$ CDM models (with or without a cosmological constant) have been computed and various fitting functions have been given (e.g., Bardeen et al. 1986 for zero-baryon models; Holtzman 1989; Efstathiou, Bond, & White 1992). But to date, no complete spectra have been published for both components in the CDM+HDM models for all cosmologically interesting ranges of parameters. Specific models have been examined, with various approximations made in the Boltzmann calculation. Holtzman (1989) compiled fitting formulas for the present-day *baryon* transfer function for $\Omega_\nu = 0.1$ and 0.3. Van Dalen & Schaefer (1992) tabulated fits to the previously computed transfer functions (Schaefer, Shafi, & Stecker 1989) for the density-weighted power spectrum at $z = 10$ for discrete values of Ω_ν between 0 and 0.53. Klypin et al. (1993) studied the $\Omega_\nu = 0.3, \Omega_b = 0.1$ model. Pogosyan & Starobinsky (1995) provided a fitting formula for the linear gravitational potential. Although the total power spectrum is useful for many linear calculations, the separate CDM and HDM spectra and the growth rate are essential, for example, for generation of initial conditions in numerical simulations. Moreover, all the Boltzmann calculations above either assumed zero baryons, which can lead to discrepancies as large as 25% for models with 5% baryons (see §2.2 below), or ignored the anisotropic stress and the higher moments in the distribution function of the massive neutrinos.

Section 2 of this paper presents analytic approximations to the linear growth rate of the density field, the CDM and HDM power spectra, the density-weighted power spectrum, and the rms mass fluctuations in spatially flat $\Omega_\nu \lesssim 0.3$ CDM+HDM models. The approximations generally differ by less than 10% from the numerically integrated results for the ranges $k \lesssim 10\,h$ Mpc^{-1}, $0 \le z \lesssim 15$, and $0.5 \lesssim h \lesssim 0.8$. The power spectra used in the fit are computed from the Boltzmann code discussed in Ma & Bertschinger (1995), which includes a careful treatment of the massive neutrino phase space and uses 50 Legendre-modes in the angular expansion of the distribution function. The calculations include CDM, baryons, photons, and one massive and two massless neutrino species. The range $0 \le \Omega_\nu \lesssim 0.3$ is chosen since it spans the standard (albeit troubled) pure CDM model ($\Omega_\nu = 0$) and the previously preferred $\Omega_\nu = 0.3$ model in the literature. Late galaxy formation due to excessive neutrino free-streaming invalidates the $\Omega_\nu = 0.3$ model (Mo & Miralda-Escude 1994; Kauffmann & Charlot 1994; Ma & Bertschinger 1994; Klypin et al. 1995), leaving $0 < \Omega_\nu < 0.3$ the only open window for the standard CDM+HDM models. Numerical simulations of COBE-normalized CDM+HDM models indicate that for an exact scale-invariant power spectrum ($n = 1$), a value of $\Omega_\nu \approx 0.2$ is needed to simultaneously satisfy the high-redshift constraint from damped Lyman-α absorbers and the zero-redshift constraint from galaxy pairwise velocity dispersions (Ma & Bertschinger 1994; Ma 1995).

In §3, linear theory, with the power spectra above as an input, is used to explore the $Q_{\rm rms-PS}$, n, h, and Ω_ν parameter space. The task of gathering observational constraints and finding a concordance region in various slices of this multi-dimensional parameter space has been performed by van Dalen & Schaefer (1992), Liddle & Lyth (1993), Pogosyan & Starobinsky (1993, 1995), and Liddle et al. (1995). The emphasis here is on physical understanding and explicit illustration of the parameter-dependence of the growth rates, the power spectra, and cluster abundance. The effect of a small tilt ($n \gtrsim 0.8$) in the primordial power spectrum on the cluster abundance is also examined. Setting the spectral index n to unity in the standard CDM and CDM+HDM models is, after all, only a simplification. Most inflationary models predict *nearly* scale-invariant spectra for the density fluctuations that have an additional logarithmic dependence on the wavenumber k. The primordial power spectrum is therefore never exactly scale-invariant, although a k-independent, $n \neq 1$ spectral index approximates the logarithmic dependence well (Crittenden & Steinhardt 1992). The intention here is to explore small deviations from the canonical $n = 1$, but not to study the models with large tilts that would require finer tuning of the inflaton potentials.

2. Analytic Approximations

The presence of massive neutrinos in CDM+HDM models complicates the computation of the power spectrum because the initially relativistic neutrinos become non-relativistic at $k_B T_\nu \sim m_\nu c^2$. This is reflected in the time-dependent energy-momentum relation: $\epsilon^2 = q^2c^2 + a^2 m_\nu^2 c^4$, where ϵ is the comoving energy, a is the expansion factor, and q denotes the magnitude of the conjugate momentum, which is a constant for free-streaming neutrinos in the absence of metric perturbations. As a result, although the q-dependence in the phase space distribution can be integrated out for massless particles in the Boltzmann calculation, the distribution of massive neutrinos must be computed on an additional grid for the momentum space. This lengthens the numerical integration time considerably, especially for large wavenumbers (see, e.g., Ma & Bertschinger 1995).

The presence of massive neutrinos also considerably complicates the procedure for fitting the power spectrum because the free streaming of the neutrinos retards the growth of the density fields, but only below the free-streaming scale. The amount of suppression depends on the redshift, the length scale, the Hubble constant, and the neutrino mass (or equivalently, Ω_ν). As a result, the linear power spectrum does not simply grow as a^2 on all length scales as in the standard CDM model, and the analytic approximations will depend on Ω_ν, h, and a in addition to the wavenumber k. The simple fitting procedure to a function $P_c(k)$ of a single variable in the CDM model therefore becomes a multi-variable problem when massive neutrinos are present.

Figure 1 shows the numerical results from our Boltzmann code (available at http://arcturus.mit.edu/cosmics/; see Bertschinger 1995 and Ma & Bertschinger 1995 for descriptions) for the present-day ($a = 1$) power spectra for the pure CDM and four CDM+HDM models. The spectral index is taken to be $n = 1$, and $H_0 = 50$ km s^{-1} Mpc^{-1}. One would perhaps first adopt the brute force approach of fitting the cold and hot spectra P_c and P_ν directly for the

ranges of k, Ω_ν, a, and H_0 of interest. However, Figure 1 shows that unlike P_c, P_ν does not vary systematically with Ω_ν for $k \gtrsim 0.5h$ Mpc^{-1}. This behavior makes it difficult to envision a simple functional form to approximate P_ν.

One solution is to fit the ratios of the power spectra rather than the spectra directly. Figures 2 and 3 show the behavior of three functions f, g, and $\mathcal{H}$ that are defined by

$$\begin{aligned} f(k,a,\Omega_\nu) &= \frac{1}{2}\frac{d\log P_c(k,a,\Omega_\nu)}{d\log a}\,, \\ P_c(k,a,\Omega_\nu) &= g(k,a,\Omega_\nu)\,P_c(k,a,\Omega_\nu=0)\,, \\ P_\nu(k,a,\Omega_\nu) &= \mathcal{H}(k,a,\Omega_\nu)\,P_c(k,a,\Omega_\nu)\,. \end{aligned} \tag{1}$$

The function $f(k,a,\Omega_\nu)$ represents the growth rate of the CDM density field, $g(k,a,\Omega_\nu)$ represents the ratio of the CDM power spectrum P_c in CDM+HDM models to that in the pure CDM model, and $\mathcal{H}(k,a,\Omega_\nu)$ represents the ratio of the power in the hot and cold components in a given model. The merit of using these functions is that they all vary systematically with Ω_ν, k, and a, as shown in Figures 2 and 3. It is therefore much easier to formulate an elegant ansatz for the analytic approximations and obtain greater accuracies for the fits.

There are still four parameters k, Ω_ν, a, and H_0 to be considered. Further simplification is achieved by identifying physical processes that introduce special length scales into the power spectrum. It is useful to first recall that the power spectrum for a pure CDM model exhibits a break at $k_{\rm eq}$, the horizon size at matter-radiation equality. Since $k_{\rm eq} \propto \Omega_m h^2$ for a model with a total matter density Ω_m, and the observable wavenumbers are in units of h Mpc^{-1}, the shape parameter $\Gamma = \Omega_m h$ can be used to characterize this single feature in the pure CDM power spectrum (Efstathiou et al. 1992). The same break should also exist in the power spectra of CDM+HDM models since the density perturbations in both components cannot grow if they enter the horizon in the radiation-dominated era. In this paper, $\Omega_m = 1$, so $\Gamma = h$.

For the CDM+HDM models, the neutrino free-streaming process introduces a second length scale in the power spectrum. The scaling of the free-streaming distance can be understood in terms of the (comoving) neutrino Jeans wavenumber $k_{\rm fs}^2 = 4\pi G\rho a^2/v_{\rm med}^2$, where $v_{\rm med}$ is taken to be the median neutrino speed in the Fermi-Dirac distribution. (See Bond & Szalay 1983 for a discussion of Jeans lengths for collisionless particles.) For $k < k_{\rm fs}$, the density perturbation in the neutrinos is Jeans unstable and grows unimpeded in the matter-dominated era; for $k > k_{\rm fs}$, the density perturbation decays due to neutrino phase mixing. When the neutrinos are relativistic, $v_{\rm med} \sim c$, and the free-streaming distance is approximately the particle horizon, which scales as $k_{\rm fs}(a) \propto a^{-1}$ (in the radiation-dominated era). The neutrinos become non-relativistic at $a \sim 3k_B T_{0\,\nu}/m_\nu c^2$ (where $T_{0\,\nu}$ is the neutrino temperature today), after which $v_{\rm med} \propto k_B T_{0\,\nu}/a m_\nu c$. The relations $m_\nu \propto \Omega_\nu h^2$ and $\rho \propto a^{-3}h^2$ then imply $k_{\rm fs}(a) \propto a^{1/2}\Omega_\nu h^3$. The decrease with time in the free-streaming distance of non-relativistic neutrinos allows neutrinos to fall into the CDM potential well and to grow with the CDM on increasingly smaller scales. This effect can be seen by comparing f and $\mathcal{H}$ in Figure 2 and 3, where both functions remain at unity to a larger k at $a = 1$

than $a = 0.1$.

Based on the reasoning above, one can simplify the dependence on the parameters a, Ω_ν, and h by introducing a second shape parameter,

$$\Gamma_\nu = a^{1/2}\Omega_\nu h^2\,, \tag{2}$$

that characterizes the effect of decreasing free-streaming distances on the power spectrum. This realization was crucial for the simplification of the functional forms and the improvement of the fits described below.

Below I describe the analytic approximations to the linear growth rate, the separate CDM and HDM power spectra, the density-weighted power spectrum, and the rms mass fluctuations. A summary of the equations and the fitting coefficients is given in Table 1.

2.1. Growth Rates

In the standard CDM model, the CDM density field δ_c grows as the expansion factor on all scales; therefore $f \equiv d\log\delta/d\log a = 1$. The massive neutrinos in CDM+HDM models introduce an additional length scale, the free-streaming distance, below which the density fluctuations are washed out and the growth rate is retarded. Consequently, the growth rates in CDM+HDM models are functions of the wavenumber k, Ω_ν, and time. This dependence is illustrated in Figures 2a and 3a.

Before searching for an analytical approximation, it is useful to ascertain first the asymptotic behavior of the function. Since HDM behaves like CDM above the free-streaming distance, $f \to 1$ as $k \to 0$. At large k where the HDM density field is negligible compared to CDM, the time evolution of the latter is governed by the linearized fluid equation $\ddot{\delta_c} + \dot{a}\dot{\delta_c}/a = 1.5H^2a^2\Omega_c\delta_c$, where the dots denote differentiation with respect to the conformal time τ. Since $Ha = 2/\tau$ in the matter-dominated era, the growing solution is easily shown to give (Bond, Efstathiou, & Silk 1980)

$$f_\infty \equiv f(k\to\infty) = \frac{1}{4}\sqrt{1+24\Omega_c} - \frac{1}{4} = \frac{5}{4}\sqrt{1-\frac{24}{25}\Omega_\nu} - \frac{1}{4}\,. \tag{3}$$

It is interesting to note that

$$f_\infty \approx \Omega_c^{0.6} \tag{4}$$

is an excellent approximation to equation (3), especially for the range $\Omega_c \gtrsim 0.7$ studied in this paper. It is sometimes convenient to express all dependence in terms of $\Omega_\nu = 1 - \Omega_c$, and

$$f_\infty \approx \Omega_c^{0.6} \approx 1 - 0.68\Omega_\nu^{1.05} \tag{5}$$

is accurate to better than 99.7% for $\Omega_\nu \lesssim 0.3$ (for both expressions).

It is *not* a coincidence that the form above is identical to the widely-used formula $f = \Omega_m^{0.6}$ for a mildly open model with matter density Ω_m: equation (3) is exact for the growth rates in open

models if Ω_c is replaced with Ω_m, and a CDM+HDM model in fact evolves like an open universe with an effective density $\Omega_c < 1$ on scales much below the neutrino free-streaming distance. Nevertheless, it should be remembered that while f is scale-independent for open models, it is scale-dependent for CDM+HDM models.

An excellent approximation to the growth rate is given by

$$f(x,\Omega_\nu) = \frac{1+\Omega_c^{0.6} a_1\, x^{a_2}}{1+a_1\, x^{a_2}}\,, \qquad x \equiv \frac{k}{\Gamma_\nu h}\,, \tag{6}$$

where $\Gamma_\nu = a^{1/2}\Omega_\nu h^2$, $\Omega_c + \Omega_\nu = 1$, and the best-fit parameters are $a_1 = 0.1161$ and $a_2 = 1.363$ for k in units of Mpc^{-1}. The fractional error of the fit relative to the numerically computed values is smaller than 0.5% for $k \lesssim 20\,h$ Mpc^{-1}, $0.05 \lesssim \Omega_\nu \lesssim 0.3$, $0.5 \lesssim h \lesssim 0.8$, and $0 \le z \lesssim 15$. The functional form is chosen to approach the asymptotic values discussed above. As promised, equation (6) depends only on the variable x that characterizes the neutrino free-streaming scale, and Ω_ν (or Ω_c) via f_∞. The solid and dashed curves in Figures 2a and 3a compare the exact and fitted growth rates at $a = 1$ and 0.1 in different CDM+HDM models with $h = 0.5$. The top panel of Figure 4 illustrates the perfect scaling with the Hubble constant through $k/\Gamma_\nu h \propto k/h^3$. The shape parameter Γ associated with matter-radiation equality discussed earlier does not affect f in the matter-dominated era of concern here.

2.2. CDM Power Spectrum

Since the strategy here is to use the ratios of the spectra, it is essential to have an accurate approximation for the power spectrum $P_c(k,a,\Omega_\nu = 0)$ in the pure CDM model as a starting point. I will adopt the functional form of Bardeen et al. (1986)

$$P_c(q,a,\Omega_\nu = 0) = a^2\, A\, k^n \left[\frac{\ln(1+\alpha_1 q)}{\alpha_1 q}\right]^2 \frac{1}{[1+\alpha_2 q + (\alpha_3 q)^2 + (\alpha_4 q)^3 + (\alpha_5\, q)^4]^{1/2}}\,, \quad q = \frac{k}{\Gamma h}\,, \tag{7}$$

where $\Gamma = \Omega_m h$ as discussed above. However, the coefficients $\alpha_1 = 2.34, \alpha_2 = 3.89, \alpha_3 = 16.1, \alpha_4 = 5.46$, and $\alpha_5 = 6.71$ from Bardeen et al. (1986) are accurate for the zero-baryon CDM model only. Increasing the baryonic fraction Ω_b decreases the power since the baryonic component cannot fall into the CDM potential wells until after recombination. Compared to the standard CDM model with $\Omega_c = 0.95$ and $\Omega_b = 0.05$, equation (7) overpredicts the power by as much as 25% at $k \gtrsim 0.1$ Mpc^{-1} (for fixed long-wavelength normalization A). A high-accuracy fit for the $\Omega_b = 0.05$ CDM model can be achieved by modifying the coefficients to $\alpha_1 = 2.205, \alpha_2 = 4.05, \alpha_3 = 18.3, \alpha_4 = 8.725$, and $\alpha_5 = 8.0$. The fractional error relative to the direct numerical result is smaller than 1% for $k < 40\,h$ Mpc^{-1}. Alternatively, replacing $\Gamma = \Omega_m h$ with $\Gamma = \exp(-2\Omega_b)\Omega_m h$ and using the Bardeen et al. coefficients in equation (7) can approximate the effect of the baryons (Peacock & Dodds 1994). This enables one to explore a wide range of Ω_b, but the error is larger for the standard $\Omega_b = 0.05$ model: $\lesssim 10\%$ compared to $\lesssim 1\%$ provided by the new coefficients above.

If the temperature fluctuations arise purely from the Sachs-Wolfe effect (Sachs & Wolfe 1967), the normalization factor A in equation (7) is related to $Q_{\rm rms-PS}$ by

$$A = k_0^{1-n} \frac{3}{20\pi} \left(\frac{2c}{H_0}\right)^4 \frac{Q_{\rm rms-PS}^2}{T_{0,\gamma}^2} = 2.689 \times 10^3 \, k_0^{1-n} \left(\frac{Q_{18}}{T_{2.726}}\right)^2 \, h^{-4} \, {\rm Mpc}^4 \,, \qquad (8)$$

where $Q_{18} \equiv Q_{\rm rms-PS}/18\,\mu K$, $T_{2.726} = T_{0,\gamma}/2.726K$, and $k_0 \approx \ell \, H_0/2c \approx 1/600\,h$ Mpc^{-1} for COBE. There are other corrections to this formula, but it is good to $\lesssim 1\%$ for $\Omega = 1$ CDM models with $h = 1$ and $\lesssim 4\%$ for h as low as 0.3 (Bunn, Scott, & White 1995; White & Bunn 1995). The best COBE value for $Q_{\rm rms-PS}$ is also model-dependent and is discussed in §3.1.

The next step is to relate the CDM power spectra P_c in models with different Ω_ν. Figures 2b and 3b illustrate the effect on P_c when CDM is partially replaced by HDM in a spatially-flat model. Since the massive neutrinos do not cluster until the neutrino temperature has dropped below their mass scale, the CDM component evolves more slowly early on with an effective $\Omega = 1 - \Omega_\nu < 1$ at k above the free-streaming scale . Consequently, the ratio $g = P_c(k, \Omega_\nu)/P_c(k, \Omega_\nu = 0)$ becomes smaller for larger Ω_ν.

The large-k behavior of g can be derived analytically from the definition of the growth rate in equation (1). It is $g(k \to \infty) \propto a^{2(f_\infty - 1)}$, where f_∞ is given by equation (3). Using $1 - f_\infty \propto \Omega_\nu^{1.05}$ as given by equation (5), I find the following functional form to give a good approximation:

$$\frac{P_c(k, a, \Omega_\nu)}{P_c(k, a, \Omega_\nu = 0)} = g(x, \Omega_\nu) = \left(\frac{1 + b_1 \, x^{b_4/2} + b_2 \, x^{b_4}}{1 + b_3 \, x_0^{b_4}}\right)^{\Omega_\nu^{1.05}} \,, \quad x = \frac{k}{\Gamma_\nu} \,, \quad x_0 = x(a = 1) \,, \qquad (9)$$

where $\Gamma_\nu = a^{1/2} \Omega_\nu h^2$, and the best-fit parameters are $b_1 = 0.01647, b_2 = 2.803 \times 10^{-5}, b_3 = 10.90$, and $b_4 = 3.259$ for k in units of Mpc^{-1}. It is important to note that x is defined to be k/Γ_ν instead of $k/\Gamma_\nu h$ as in equation (6). This results from the fact that the two shape parameters $\Gamma = h$ ($\Omega_m = 1$ in this paper) and $\Gamma_\nu = a^{1/2} \Omega_\nu h^2$ discussed earlier depend on different powers of the Hubble constant, and both parameters affect the shape of g, which involves P_c from two different models. Since the free-streaming wavenumber $k_{\rm fs}$ is much larger than $k_{\rm eq}$ at the redshifts of concern here ($z \lesssim 20$), $\Gamma \propto h$ tends to control the scaling with h in the region where g starts to deviate from unity in Figures 2 and 3, while $\Gamma_\nu \propto h^2$ controls the scaling with h at larger k. This mixed dependence on h causes potential complication for the fitting formula. For the range $0.5 \lesssim h \lesssim 0.8$ and $k \lesssim 10\,h$ Mpc^{-1} of interest here, however, I find that the scaling $x \propto k/h^2$ works fairly well, as illustrated by the middle panel of Figure 4. Therefore, x is modified to depend on one less power of h than for the function f to account for the effect of Γ. The error in P_c in equation (9) relative to the numerically computed values is $\lesssim 10\%$ for $k \lesssim 10\,h$ Mpc^{-1}, $0.05 \lesssim \Omega_\nu \lesssim 0.2$, $0.5 \lesssim h \lesssim 0.8$, and $0 \le z \lesssim 15$. For $\Omega_\nu \approx 0.3$, the error is still $\lesssim 10\%$ for $h = 0.5$ and $k \lesssim 10\,h$ Mpc^{-1}, but it increases to $\sim 20\%$ for $h = 0.8$ at high k.

2.3. HDM Power Spectrum

The HDM to CDM ratio $\mathcal{H}(k,\Omega_\nu)$ decreases monotonically with decreasing Ω_ν as shown by Figures 2c and 3c. This trend is caused by the longer neutrino free-streaming lengths for smaller neutrino masses (hence smaller Ω_ν), which makes $\mathcal{H}$ deviate from unity at smaller k. As discussed earlier, the dependence of P_ν/P_c on k, a, Ω_ν and H_0 can be combined in a single variable x that characterizes the neutrino free streaming distance. A good analytic approximation is given by

$$\frac{P_\nu(k,a,\Omega_\nu)}{P_c(k,a,\Omega_\nu)} = \mathcal{H}(x) = \frac{e^{-c_1 x}}{1 + c_2 x^{1/2} + c_3 x + c_4 x^{3/2} + c_5 x^2}\,, \qquad x \equiv \frac{k}{\Gamma_\nu h}\,, \tag{10}$$

where $\Gamma_\nu = a^{1/2}\Omega_\nu h^2$, and $c_1 = 0.0015, c_2 = -0.1207, c_3 = 0.1015, c_4 = -0.01618$ and $c_5 = 0.001711$. The resulting P_ν has an error $\lesssim 15\%$ relative to the numerical results for $k \lesssim 10\,h$ Mpc^{-1}, $0.05 \lesssim \Omega_\nu \lesssim 0.3$, $0.5 \lesssim h \lesssim 0.8$, and $0 \le z \lesssim 15$.

The bottom panel of Figure 4 illustrates the perfect scaling of $\mathcal{H}$ with $x \propto k/h^3$. The complication due to different h-scalings in the function g (see §2.2) does not arise here because the physical process associated with shape parameter $\Gamma = h$ introduces breaks in P_c and P_ν at the same length scale (i.e., at $k_{\rm eq}$), and the effect interestingly cancels out in the ratio $\mathcal{H}$.

2.4. Density-Weighted Power Spectrum

Although the clustering of the cold and hot components is described by the separate power spectra P_c and P_ν discussed above, it sometimes is useful to have an analytic approximation to the density-weighted power spectrum $P(k) = \{\Omega_\nu P_\nu^{1/2} + (1-\Omega_\nu)P_c^{1/2}\}^2$ that measures the total gravitational fluctuations contributed by the separate components. Here I have assumed that CDM and baryons have the same power (i.e., $P_c = P_b$), which is a very good approximation for the range of redshifts and Ω_b studied in this paper. The functional form used for the CDM spectrum P_c in equation (9) works well here, and a good approximation is given by

$$P(k,a,\Omega_\nu) = P_c(k,a,\Omega_\nu = 0)\left(\frac{1 + d_1\, x^{d_4/2} + d_2\, x^{d_4}}{1 + d_3\, x_0^{d_4}}\right)^{\Omega_\nu^{1.05}}\,, \quad x = \frac{k}{\Gamma_\nu}\,, \quad x_0 = x(a=1)\,, \tag{11}$$

where $P_c(k,a,\Omega_\nu = 0)$ for the pure CDM model is given by equation (7), and $d_1 = 0.004321, d_2 = 2.217\times10^{-6}, d_3 = 11.63$, and $d_4 = 3.317$. The error in the resulting P relative to the numerically computed values is $\lesssim 10\%$ for the ranges $k \lesssim 20\,h$ Mpc^{-1}, $0.05 \lesssim \Omega_\nu \lesssim 0.3$, $0.5 \lesssim h \lesssim 0.8$, and $0 \le z \lesssim 15$.

Pogosyan & Starobinsky (1995) introduced a more complicated 8-parameter fitting formula for the gravitational potential that gives results similar to ours. The analytic approximation provided by Efstathiou et al. (1992), however, does not fit the density-weighted CDM+HDM $P(k)$ well. Their formula $P(k) = Bk/\{1 + [ak + (bk)^{3/2} + (ck)^2]^\nu\}^{2/\nu}$, with $a = 6.4/(\Gamma h)$ Mpc, $b = 3.0/(\Gamma h)$ Mpc, $c = 1.7/(\Gamma h)$ Mpc, $\nu = 1.13$, and $\Gamma = 0.2(\Omega_\nu/0.3)^{-0.5}$ does not take into

account the redshift dependence of the shape and does not have the correct dependence on Ω_ν at large k. It produces too little power at $0.01 \lesssim k \lesssim 1$ Mpc^{-1} by as much as a factor of ~ 2. On the other hand, this formula with $\Gamma = \Omega_m h = 0.5$ works fairly well for the $\Omega_b = 0.05, h = 0.5$ flat CDM model. The maximal discrepancy is $\sim 18\%$, compared to 25% in the original Bardeen et al. fits.

2.5. Mass Fluctuations σ

The linear rms mass fluctuations in spheres of radius R are related to the power spectrum P by

$$\sigma^2(R, \Omega_\nu, a) = \int_0^\infty \frac{dk}{k}\, 4\pi k^3 P(k, \Omega_\nu, a) W^2(kR)\,, \tag{12}$$

where $W(x) = 3(\sin x - x\cos x)/x^3$ is the tophat window function, and the mass enclosed in the sphere is $M = 4\pi\rho_0 R^3/3$, with ρ_0 denoting the background mass density of the universe. Although different filter windows have been used in the literature, and there is no *a priori* reason to prefer a particular window function, Lacey & Cole (1994) find that the tophat gives the best fit to N-body simulations with initial power-law $P(k)$. More importantly, the best-fit δ_c for a tophat is insensitive to the spectral index n. In contrast, they find the best fit δ_c to depend more strongly on n when the Gaussian window is used. Ma & Bertschinger (1994) also find the shapes of the Press-Schechter mass functions computed with the tophat filter to give a better match in CDM+HDM simulations. Since a family of models with different spectral shapes at large k is being studied here, the tophat window will be the most robust filter.

Figure 5 shows the present-day $\sigma(R, \Omega_\nu)$ for $n = 1$ and $h = 0.5$ models with different Ω_ν. At large R, all curves converge because the same 4-year COBE normalization ($Q_{\rm rms-PS} = 18\,\mu K$) is used, and $\sigma \propto R^{(-3-n)/2}$ since $P(k) \propto k^n$ at small k. The small-R behavior simply reflects the effect of neutrino free streaming on the power spectrum. I will again fit to $\sigma(\Omega_\nu = 0)$ for the pure CDM model and then the ratios $\sigma(\Omega_\nu)/\sigma(\Omega_\nu = 0)$. An excellent analytic approximation to $\sigma(\Omega_\nu = 0)$ is given by

$$\sigma(R, \Omega_\nu = 0) = Q_{18}\; h^2 \left(\frac{R}{R_0}\right)^{(1-n)/2} \frac{1}{a_1 + a_2\, x^{a_4} + a_3\, x^2}\,, \qquad x \equiv Rh^2\,, \tag{13}$$

where $Q_{18} = Q_{\rm rms-PS}/18\,\mu K, a_1 = 0.01359, a_2 = 0.05541, a_3 = 0.001702, a_4 = 0.8032$, $R_0 = 1000$ Mpc, and R is in units of Mpc. The exponent $(1-n)/2$ is chosen so that $\sigma \propto R^{(-3-n)/2}$ at large R. The fractional error is $\lesssim 5\%$ for $R = 0.07$ – $350\ h^{-1}$ Mpc, or $M = 4 \times 10^8$ – $5 \times 10^{19} h^{-1} M_\odot$. For CDM+HDM models, one can use

$$\sigma(R, \Omega_\nu) = \sigma(R, \Omega_\nu = 0)\, \frac{1 + \Omega_c^{a_3} a_1\, x^{a_2}}{1 + a_1\, x^{a_2}}\,, \qquad x \equiv R\Gamma_\nu\,, \tag{14}$$

where $\Gamma_\nu = \Omega_\nu h^2$, $\Omega_c = 1 - \Omega_\nu$, and the best-fit parameters are $a_1 = 0.7396, a_2 = -0.8927$, and $a_3 = 5.106$. The fractional error is $\lesssim 10\%$. The result of the fitting is shown in Figure 5 (as dashed curves).

As emphasized earlier, the shape of $P(k, a, \Omega_\nu)$ has a non-trivial dependence on the redshift due to neutrino free streaming. However, the mass fluctuations obey $\sigma(R, \Omega_\nu, a) = a\,\sigma(R, \Omega_\nu, a = 1)$ to a good approximation, with <10% error for $M \gtrsim 10^{10} M_\odot$ (see Figure 5). I therefore will not give a time-dependent approximation. If σ is required to higher precision, or at a lower mass, one can carry out the simple integral in equation (12) using the analytic approximation for $P(k, a, \Omega_\nu)$ in equation (11).

3. Observational Constraints

3.1. Reconstructed $P(k)$

The theoretical linear power spectra computed above can be put to the test against the observed power spectra of galaxies and clusters, if the effects of non-linear evolution, redshift-space distortions, and bias are corrected for. This is not a straightforward task, especially on highly nonlinear scales. By limiting the study to the quasi-linear regime ($k \lesssim 0.5\,h$ Mpc^{-1}), Peacock & Dodds (1994) attempted to reconstruct the linear mass power spectrum from eight independent sets of data from optical, radio, and IRAS galaxies and optical and radio Abell clusters. They were able to obtain good internal agreement for the estimated power spectrum given specific conditions: a significant redshift-space distortion; a scale-independent bias for a given class of objects, with relative bias factors for Abell clusters, radio galaxies, optical galaxies, and IRAS galaxies required to be 4.5 : 1.9 : 1.3 : 1 to within 6% rms. Among the pure CDM models parameterized by the shape parameter $\Gamma = \Omega_m h$ (see eq. [7]), the best fit was found to be given by $\Gamma \approx 0.25$.

Figure 6 compares the final estimate for the linear power spectrum from Peacock & Dodds (1994) with those for the standard CDM and three CDM+HDM models with $h = 0.5$ computed in the previous section. (The density-averaged $P = \{\Omega_\nu P_\nu^{1/2} + (1-\Omega_\nu) P_c^{1/2}\}^2$ is used for CDM+HDM models.) Three primordial spectral indices $n = 1$, 0.95, and 0.9 are shown. The bottom two panels illustrate the effect of tensor contributions in the tilted models. Whether a model produces a non-zero tensor fluctuation depends on the shape of the inflaton potential at the time of the first horizon crossing (60 or so e-folds before the end of inflation). Inflationary models, such as the extended or chaotic models, generally give a tensor-to-scalar ratio of $T/S \approx 7(1-n)$ (Davis et al. 1992), although the so-called natural inflationary model predicts a negligible tensor contribution (Adams et al. 1993). Since COBE measures the combined scalar and tensor anisotropies, the effect of a non-zero tensor mode, when the tilt is small, is to lower the normalization for the scalar power spectrum by $S/(S+T)$ for a given $Q_{\rm rms-PS}$.

An additional effect on the normalization that must be considered is the dependence of $Q_{\rm rms-PS}$ on parameters such as n, Ω_b and h assumed in a given model. The dependence arises because there exist small corrections to the Sachs-Wolfe effect (Sachs & Wolfe 1967) that is the main contributor to the angular power spectrum for the temperature fluctuations in the cosmic microwave background on the COBE scale. A detailed analysis of such dependence has been

carried out by Bunn et al. (1995), who obtain $Q_{\rm rms-PS}(n) = 21.1 \exp[0.69(1-n)]\,\mu K$ from the 2-year COBE data (for a pure Sachs-Wolfe spectrum). A maximum likelihood analysis of the same data by Gorski et al. (1994) finds $Q_{\rm rms-PS}(n) = (39+2n)\exp(-0.73n)$ with quadrupole, and $Q_{\rm rms-PS}(n) = (40+2n)\exp(-0.74n)$ without quadrupole. Results from the 4-year COBE data have been announced recently (Gorski et al. 1996; Bennett et al. 1996). I therefore will use the latest value $Q_{\rm rms-PS} = 18\,\mu K$ for $n = 1$ (Gorski et al. 1996), and $Q_{\rm rms-PS} = 19.2\,\mu K$ and $20.5\,\mu K$ for $n = 0.9$ and 0.8 (Gorski, private communication), respectively. (Note that using $Q_{\rm rms-PS}(1) = 18$ instead of 21.1 in the Bunn et al. formula gives very similar results: $Q_{\rm rms-PS} = 19.3\,\mu K$ for $n = 0.9$ and $20.7\,\mu K$ for $n = 0.8$.) The dependence on n for $n = 0.8 - 1$ is weak, but it is taken into account in Figure 6. Varying Ω_b from 0.01 to 0.1 in the CDM model changes $Q_{\rm rms-PS}$ by only about 1% (Bunn et al. 1995), so it will not be considered here.

As Figure 6 illustrates, the 4-year COBE result is consistent with the amplitude of reconstructed power spectrum at small k, but all $n = 1$ models with $0 \le \Omega_\nu \le 0.3$ normalized to this value have too much power at $0.05 \lesssim k \lesssim 0.2\,h\,{\rm Mpc}^{-1}$. A slight tilt of $n = 0.9 - 0.95$ brings the CDM+HDM models into excellent agreement with the data. For a given COBE normalization, the power spectrum of a tilted model with a negligible T/S (bottom panel of Fig. 6) has a higher amplitude than that of a model with $T/S \approx 7(1-n)$ (middle panel); therefore a slightly smaller n is generally needed to match the reconstructed power spectrum. Figure 6 shows that the four highest k points in Peacock & Dodds (1994) favor $\Omega_\nu \approx 0.1 - 0.2$, although Liddle et al. (1995) recently questioned the validity of these high-k points. It is also interesting to note that the spectra for the $\Omega_\nu = 0.1$ model with $n = 0.95$ (with tensor) and $n = 0.9$ (without tensor) are very similar to the open CDM spectrum with $\Gamma = 0.25$.

Figure 7 shows the effect of increasing h to 0.65. The discrepancy worsens for $n = 1$, but a larger tilt of $n \approx 0.9$ (with tensor) or $n \approx 0.8$ (without tensor) can compensate for the increased power and bring the models with $\Omega_\nu \sim 0.1 - 0.3$ into good agreement with the data points.

3.2. σ_8 and Cluster Abundance

The rms linear mass fluctuation on scales of $8h^{-1}$ Mpc, σ_8, has played a very special role in the literature. Because the observed rms galaxy count on this scale is about unity (Davis & Peebles 1983), σ_8 was used to define the "bias factor", $b = \sigma_8^{-1}$, between mass and galaxies. It was also a common practice to use σ_8 for the normalization of the linear matter power spectrum, a value undetermined by most theories. After COBE, the rms quadrupole inferred from the cosmic microwave background anisotropy is often used to fix the normalization of the (matter) power spectrum. The corresponding σ_8 in a given cosmological model then depends on the shape of the power spectrum. Analytic approximations to $\sigma(R)$ have already been given by equations (13) and (14). Using $R = 8h^{-1}$ Mpc gives the following approximation for σ_8:

$$\sigma_8(\Omega_\nu = 0) = Q_{18}\,\frac{h^2\,0.008^{(1-n)/2}}{0.0136 + 0.294\,h^{0.803} + 0.109h^2}\,,$$

$$\sigma_8(\Omega_\nu) = \sigma_8(\Omega_\nu = 0)\,\frac{1+\Omega_c^{5.11}\,0.116\,(\Omega_\nu\,h)^{-0.893}}{1+0.116\,(\Omega_\nu\,h)^{-0.893}}\,, \tag{15}$$

where $Q_{18} = Q_{\rm rms-PS}/18\,\mu K$.

The masses and abundances of rich clusters of galaxies provide an independent constraint on σ_8. Evrard (1989) obtained $\sigma_8 \sim 0.5 - 0.7$ in the standard CDM model from high velocity dispersion clusters. Henry & Arnaud (1991) obtained $\sigma_8 = 0.59 \pm 0.02$ for scale-free spatially-flat models from their X-ray cluster temperature function. White, Efstathiou and Frenk (1993) found $\sigma_8 \sim 0.52 - 0.62$ for the standard CDM model using the Henry & Arnaud cluster data and the Press-Schechter (1974) approximation (assuming a linear overdensity of $\delta_c = 1.68$). Liddle et al. (1996) used the same data and also took into account the redshift dependence in the relation between cluster virial masses and temperatures. They considered both open and flat CDM models and found $\sigma_8 = 0.59^{+.21}_{-.16}$ after allowing $1.6 \le \delta_c \le 1.8$.

Here I use the Press-Schechter approximation (1974) to investigate the constraint imposed on the neutrino fraction Ω_ν in CDM+HDM models by the cluster data. The comoving number density of objects of mass above M at redshift z is given by

$$N(M,z) = \int_{\ln M}^{\infty} d\ln M' \sqrt{\frac{2}{\pi}}\frac{\rho_0(z)}{M'}\frac{\delta_c}{\sigma(M',z)}\left|\frac{d\ln\sigma}{d\ln M'}\right|\exp\left[-\frac{\delta_c^2}{2\sigma^2(M',z)}\right]\,, \tag{16}$$

where $\rho_0(z)$ denotes the background mass density of the universe, and δ_c is a free parameter characterizing the linear overdensity at the onset of gravitational collapse. The dependence on cosmological models is via $\sigma(M)$, which is given by equations (13) and (14) with $M = 4\pi R^3\,\rho_0/3$.

White et al. (1993a) approximate $\sigma(M)$ in the CDM model as a single power-law for the cluster mass range. As Figure 5 illustrates, this is not a good approximation for CDM+HDM models because $\sigma(M)$ turns over more sharply around 10^{14}–$10^{15} M_\odot$ due to the smaller power in $P(k)$. Liddle et al. (1995, 1996) adopted an improved approximation as a function of $\Gamma = \Omega_m h$ for open and flat CDM models, but they did not give a formula for $\sigma(\Omega_\nu)$ for CDM+HDM models. To compute the number density $N(M)$, one should use either σ computed from $P(k)$ in equation (11) or the analytic σ given by equations (13) and (14) above.

Figure 8 shows the present-day number density of cluster-scale objects as a function of mass for various models. Dependence of the cluster number density on the overdensity δ_c, normalization $Q_{\rm rms-PS}$, and spectral index n is also illustrated. The sensitivity to the parameters arises because cluster masses reside in the Gaussian tails of the Press-Schechter curves. Our experience with N-body simulations is that the best-fit δ_c can range from 1.68 to 1.8 (Ma & Bertschinger 1994), so both values are shown for comparison.

Figure 9 illustrates two effects that would help to lower the predicted $N(>M)$: decreasing $Q_{\rm rms-PS}$ or increasing Ω_b. The value $Q_{\rm rms-PS} = 16.4\,\mu K$ is the lower 1-σ normalization given in Bennett et al. (1996). The high value of $\Omega_b = 0.1$ (for $h = 0.5$) is preferred if the recent measurement of the deuterium to hydrogen ratio in a quasar absorption line system (Tytler, Fan,

& Burles 1996) is accurate and reflects the primordial value. Another possibility not studied here is dividing the contribution of massive neutrinos to Ω_ν among two or more species (Primack et al. 1995). For a fixed Ω_c, the longer free streaming distance of the lighter neutrinos helps to lower the power spectrum slightly and therefore gives a lower $N(> M)$.

The two data points in Figures 8 and 9 indicate the number densities of clusters with X-ray temperatures exceeding $k_BT = 3.7$ and 7 keV from Henry & Arnaud (1991). The mass range shown for the $k_BT > 3.7$ keV clusters is taken from White et al. (1993a), where the upper limit $5.5 \times 10^{14} h^{-1} M_\odot$ was estimated from cluster velocity dispersions assuming an isotropic distribution, while the lower limit $4.2 \times 10^{14} h^{-1} M_\odot$ was converted from the X-ray temperature assuming an isothermal gas and a density profile of $\rho \propto r^{-2}$. Both values correspond to masses within one Abell radius 1.5 h^{-1} Mpc and are extrapolated from the observed values at $\sim 0.5 h^{-1}$ Mpc. The mass range plotted for the $k_BT > 7$ keV clusters is from the more recent analysis of Liddle et al. (1996), who used the hydrodynamical simulations by White et al. (1993b) to calibrate the cluster masses within one Abell radius for a given X-ray temperature. Using the density profile $\rho \propto r^{-2.4}$ (White et al. 1993b), Liddle et al. then converted the mass above to the virial mass $(1.2^{+0.7}_{-0.5}) \times 10^{15} h^{-1} M_\odot$ for a cluster with a mean X-ray temperature of 7 keV in a critical-density universe.

In comparison with these published values, Figure 8 indicates that all $Q_{\rm rms-PS} = 18\,\mu K$, $n = 1$ models with $\Omega_\nu \lesssim 0.3$ and $\Omega_b = 0.05$ overpredict the cluster number density for $\delta_c = 1.68$–1.8. Models with $n = 0.9 - 0.95$ agree better, with the preferred range of Ω_ν dependent on the value of δ_c and whether or not there is a tensor contribution. Figure 8 shows the same tilted models as in Figure 6. For $n = 0.9$ and no tensor mode (normalized to $Q_{\rm rms-PS} = 19.2\,\mu K$), the preferred range is $0.2 \lesssim \Omega_\nu \lesssim 0.4$, or $0.65 \lesssim \sigma_8 \lesssim 0.8$, for $\delta_c = 1.68$ – 1.8. For $n = 0.95$ and $T/S = 7(1-n)$ (with $Q_{\rm rms-PS} = 18.5\,\mu K$), the allowed range is $0.1 \lesssim \Omega_\nu \lesssim 0.3$, or $0.6 \lesssim \sigma_8 \lesssim 0.7$. This preference for $n \approx 0.9 - 0.95$ is consistent with the conclusion drawn from the reconstructed power spectrum in the previous section. A lower $Q_{\rm rms-PS}$ or higher Ω_b in $n = 1$ models also helps to decrease the cluster number density, but the effects are smaller (see Fig. 9).

It should be kept in mind that the mass ranges adopted by White et al. (1993a) and Liddle et al. (1995, 1996) are obtained under specific assumptions. Cluster mass determination is by no means a settled issue. Temperature gradients, substructure, and ellipticity can all affect the X-ray mass estimates (see, e.g., Tsai, Katz, & Bertschinger 1994). Cluster mass function has also been estimated from velocity dispersions of cluster galaxies (e.g., Biviano et al. 1993), but inclusion of substructure in the analysis lowers the normalization (Bird 1995). We can invert the problem and ask what cluster mass is needed for the currently favored $n = 1$ CDM+HDM models to produce the observed cluster abundance. Within the narrow window $\Omega_\nu \sim 0.1$ – 0.2 allowed by both the low- and high-redshift constraints (Ma & Bertschinger 1994; Ma 1995), Figure 8 indicates that the 3.7 and 7 keV clusters would have to have a median mass of $\sim 1 - 1.5 \times 10^{15}$ and $\sim 2 - 4 \times 10^{15} h^{-1} M_\odot$, respectively, for $\Omega_\nu = 0.1$ – 0.2 models ($n = 1$) to produce the observed cluster abundance. This seems very unlikely, given that the hottest and most luminous

X-ray cluster Abell 2163 ($k_BT = 12 - 15$ keV) is recently estimated to have a mass of only $M_A = 1.07 \pm 0.13 \times 10^{15} h^{-1} M_\odot$ out to the Abell radius (Markevitch et al. 1996). For a power-law density profile $\rho(r) \propto r^{-\alpha}$ at the outer part of the cluster, this translates to a virial mass of $M_V \approx 1.5^{(3/\alpha-1)} M_A$, that is, only about $1.2 - 1.35 \times 10^{15} h^{-1} M_\odot$ for α ranging from 2.4 from simulations (White et al. 1993b) to the isothermal $\alpha = 2$.

4. Conclusions

This paper presents numerical results and analytical approximations to the linear power spectrum and the density field growth rate for a class of CDM+HDM models with neutrino fraction $\Omega_\nu \lesssim 0.3$ (neutrino mass $m_\nu \lesssim 7$ eV) that are currently of much cosmological interest. The models with $\Omega_\nu = 0$ (i.e. the standard CDM) and $\Omega_\nu \gtrsim 0.3$ have difficulty explaining various observations, leaving the range of the neutrino masses studied in the paper as the only hope for the standard CDM+HDM models. The analytical functions given by equations (6)-(11) and (13) and (14) in this paper give accurate approximations to the linear growth rate, the separate cold and hot power spectra, the density-weighted power spectrum, and the rms mass fluctuations for $k \lesssim 20\,h$ Mpc^{-1}, $z \lesssim 15$, and $0.5 \lesssim h \lesssim 0.8$ in CDM+HDM models with $\Omega_\nu \lesssim 0.3$. They should be useful as the input for most linear calculations and for the initial conditions of numerical simulations of structure formation in these models.

It is shown that the difference in the growth rate and the power spectrum between the CDM+HDM and the standard CDM models can be entirely characterized by the free-streaming distance of the neutrinos. A shape parameter $\Gamma_\nu = a^{1/2}\Omega_\nu h^2$ is introduced to explain the behavior of the power spectra in Figure 1; it also helps to greatly simplify the functional forms of equations (6), (9), and (10), and to improve the accuracy of the fits.

Linear calculations with these power spectra as input are performed to study the dependence of cluster abundance on the spectral index n, normalization $Q_{\rm rms-PS}$, tensor-to-scalar ratio T/S, baryon fraction Ω_b, and neutrino masses in $\Omega_\nu \lesssim 0.3$ models. The theoretical predictions are compared to the reconstructed $P(k)$ by Peacock & Dodds (1994) and the X-ray cluster abundance and masses from Henry & Arnaud (1991). These tests are chosen because the linear theory (with proper calibration for the clusters) should be adequate on such large scales. When normalized to the 4-year COBE $Q_{\rm rms-PS} = 18\,\mu K$, all $n = 1$, $\Omega_b = 0.05$, $\Omega_\nu \lesssim 0.3$ models predict too much power by up to a factor of ~ 2 when compared to Peacock & Dodds (1994) and Herny & Arnaud (1991). A lower $Q_{\rm rms-PS}$ or higher Ω_b both helps to reduce the discrepancy. Also considered is a slight tilt of $n = 0.9 - 0.95$ in the power spectrum, which brings the theoretical predictions into good agreement with data.

Due to the heterogeneous nature of the Peacock & Dodds sample and the uncertainties in cluster abundance and mass, it is difficult to attach a meaningful statistical significance to the validity of the various models studied in this paper. It should also be kept in mind that the

conclusion that the $n = 0.9 - 0.95$ models provide a closer match to the data depends on several implicit assumptions. These include the scale-independent bias used in Peacock & Dodds (cf. Cen & Ostriker 1992) and the isothermal and spherical model for clusters used in White et al. (1993a) and Liddle et al. (1996) to convert X-ray temperature into virialized mass. These are obviously simplifications, but modeling the deviations from such assumptions would require the introduction of parameters that can not be well determined by current data. Nonetheless, the theoretical calculations carried out in this paper should provide useful predictions that can be tested by future data.

The author is grateful to Ed Bertschinger and Peter Goldreich for valuable discussions, Una Hwang, Mark Metzger, HouJun Mo, Paul Steinhardt, and Ned Wright for helpful comments, and K. Gorski and Richard Mushotzky for useful information. Parts of the Boltzmann calculations were performed at the National Center for Supercomputing Applications. Support from a PMA Division Fellowship at Caltech is acknowledged.

Table 1. Summary of Analytic Approximations

Symbol	Equation	Coefficients 1	2	3	4	5
f	(6)	0.1161	1.363			
$P_c(\Omega_\nu = 0)$	(7)[a]	2.34	3.89	16.1	5.46	6.71
	(7)[b]	2.205	4.05	18.3	8.725	8.0
$P_c(\Omega_\nu)$	(9)	0.01647	2.803e-5	10.9	3.259	
$P_\nu(\Omega_\nu)$	(10)	0.0015	-0.1207	0.1015	-0.01618	0.001711
$P(\Omega_\nu)$	(11)[c]	0.004321	2.217e-6	11.63	3.317	
$\sigma(\Omega_\nu = 0)$	(13)	0.01359	0.05541	0.001702	0.8032	
$\sigma(\Omega_\nu)$	(14)	0.7396	-0.8927	5.106		

[a]For zero baryons, or modify variable Γ in eqn. (7) for general baryon fraction (see text)

[b]High accuracy fit (with $\lesssim 1\%$ error) for the standard CDM model with 5% baryons

[c]Density-weighted spectrum $P = \{\Omega_\nu P_\nu^{1/2} + (1 - \Omega_\nu) P_c^{1/2}\}^2$

REFERENCES

Adams, F. C., Bond, J. R., Freese, K., Frieman, J. A., & Olinto, A. V. 1993, Phys. Rev. D47, 426

Bardeen, J. M., Bond, J. R., Kaiser, N., & Szalay, A. S. 1986, ApJ, 304, 15

Bennett, D. et al. 1996, astro-ph/9601067

Bertschinger, E. 1995, astro-ph/9506070

Bird, C. M. 1995, ApJ, 445, L81

Biviano, A., Girardi, M., Giuricin, G., Mardirossian, F., & Mezzetti, M. 1993, ApJ, 411, L13

Bond, J. R., Efstathiou, G., & Silk, J. 1980, Phys. Rev. Lett., 45, 1980

Bond, J. R., & Szalay, A. S. 1983, ApJ, 274, 443

Bunn, E. F., Scott, D., & White, M. 1995, ApJ, 441, L9

Cen, R., & Ostriker, J. P. 1992, ApJ, 399, L113

Crittenden, R., & Steinhardt, P. J. 1992, Phys. Lett., B293, 32

Davis, M., & Peebles, P. J. E. 1983, ApJ, 267, 465

Davis, R. L., Hodges, H. M., Smoot, G. F., Steinhardt, P. J., and Turner, M. S. 1992, Phys. Rev. Lett., 69, 1856 (erratum 70, 1733)

Efstathiou, G., Bond, J. R., & White, S. D. M. 1992, MNRAS, 258, 1p

Evrard, A. E. 1989, ApJ, 341, L71

Gorski, K. M. et al. 1994, ApJ, 430, L89

Gorski, K. M. et al. 1996, astro-ph/9601063

Henry, J. P., & Arnaud, K. A., 1991, ApJ, 372, 410

Holtzman, J. A. 1989, ApJS, 71, 1

Kauffmann, G., & Charlot, S. 1994, ApJ, 430, L97

Klypin, A., Holtzman, J. A., Primack, J. R., & Regos, E. 1993, ApJ, 416, 1

Klypin, A., Borgani, S., Holtzman, J. A., Primack, J. R. 1995, ApJ, 444, 1

Lacey, C., & Cole, S. 1994, MNRAS, 271, 676

Liddle, A. R., & Lyth, D. H. 1993, MNRAS, 265, 379

Liddle, A. R., Lyth, D. H., Schaefer, R. K., Shafi, Q., & Viana, P. 1995, preprint, astro-ph/9511057

Liddle, A. R., Lyth, D. H., Roberts, D., & Viana, P. 1996, MNRAS, 278, 644

Ma, C.-P. 1995, in *Dark Matter*, ed. S. Holt, & C. L. Bennett (American Institute of Physics, Washington), p. 420

Ma, C.-P., & Bertschinger, E. 1994, ApJ, 434, L5

Ma, C.-P., & Bertschinger, E. 1995, ApJ, 455, 7

Markevitch, M., Mushotzky, R., Inoue, H., Yamashita, K., Furuzawa, A., & Tawara, Y. 1996, ApJ, 456, 437

Mo, H. J., & Miralda-Escude, J. 1994, ApJ, 430, L25

Peacock, J. A., & Dodds, S. J. 1994, MNRAS, 267, 1020

Pogosyan, D. Yu., & Starobinsky, A. A. 1993, MNRAS, 265, 507

Pogosyan, D. Yu., & Starobinsky, A. A. 1995, ApJ, 447, 465

Press, W. H., & Schechter, P. 1974, ApJ, 187, 425

Primack, J. R., Holtzman, J., Klypin, A., & Caldwell, D. O. 1995, Phys. Rev. Lett. 74, 2160

Sachs, R. K., & Wolfe, A. M. 1967, ApJ, 147, 73

Schaefer, R. K., Shafi, Q., & Stecker, F. W. 1989, ApJ, 347, 575

Tsai, J. C., Katz, N., & Bertschinger, E. 1994, ApJ, 423, 553

Tytler, D., Fan, X, Burles, S. 1996, astro-ph/9603069

van Dalen, T., & Schaefer, R. K. 1992, ApJ, 398, 33

White, M., & Bunn, E. F. 1995, ApJ, 450, 477

White, S. D. M., Efstathiou, G., & Frenk, C. S. 1993a, MNRAS, 262, 1023

White, S. D. M., Navarro, J. F., Evrard, A. E., & Frenk, C. S. 1993b, Nature, 366, 429

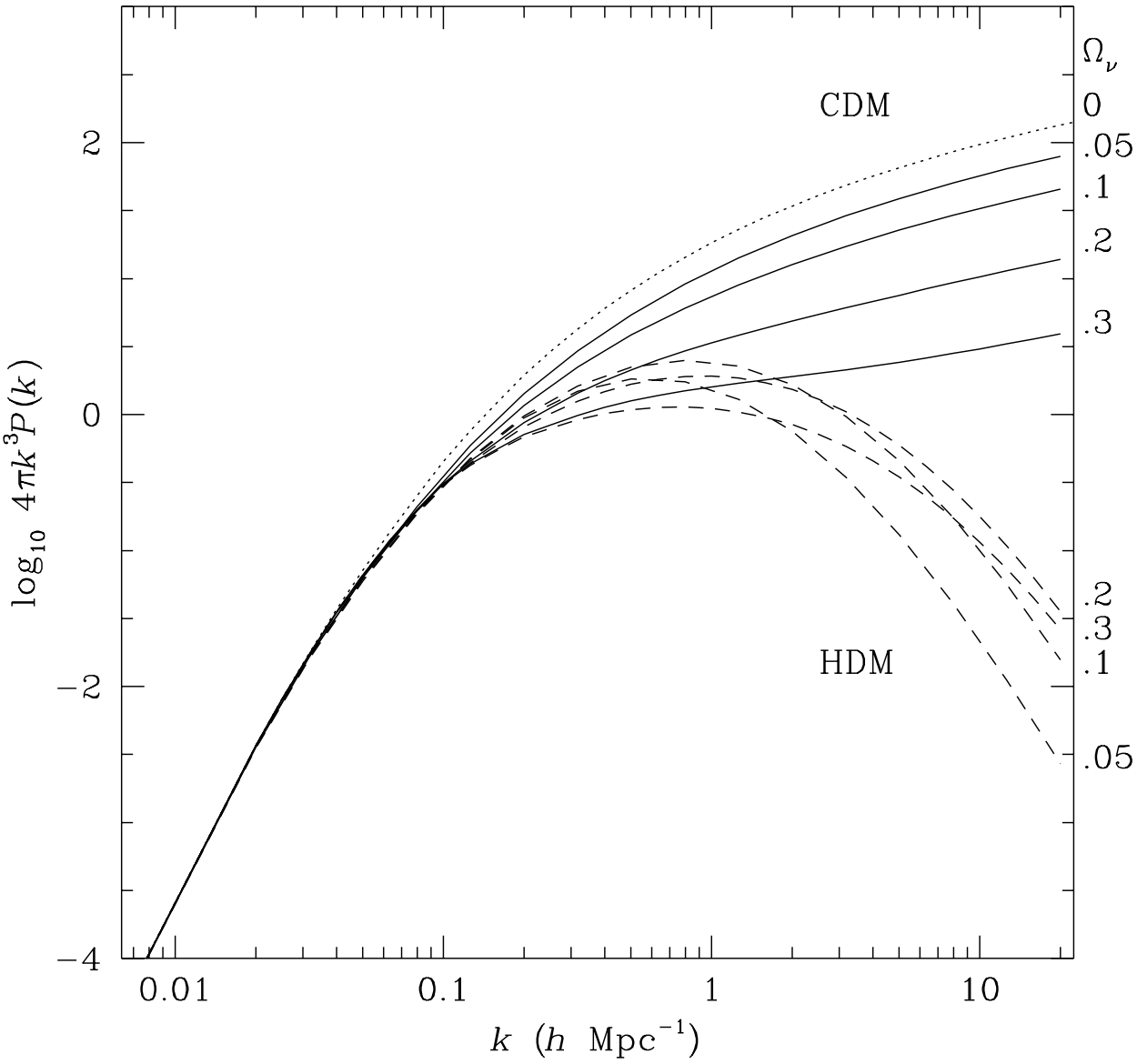

Fig. 1.— Present-day linear power spectra for the standard CDM model (dotted) and four CDM+HDM models with $n = 1$, Ω_b, and $H_0 = 50$ km s^{-1} Mpc^{-1}, computed from integrations of the Boltzmann equations. The four CDM+HDM models have $\Omega_\nu = 0.05, 0.1, 0.2$, and 0.3, and the power in the cold (solid) and hot (dashed) components are shown separately. All are normalized to the 4-year COBE result $Q_{\rm rms-PS} = 18\,\mu K$ (Gorski et al. 1996).

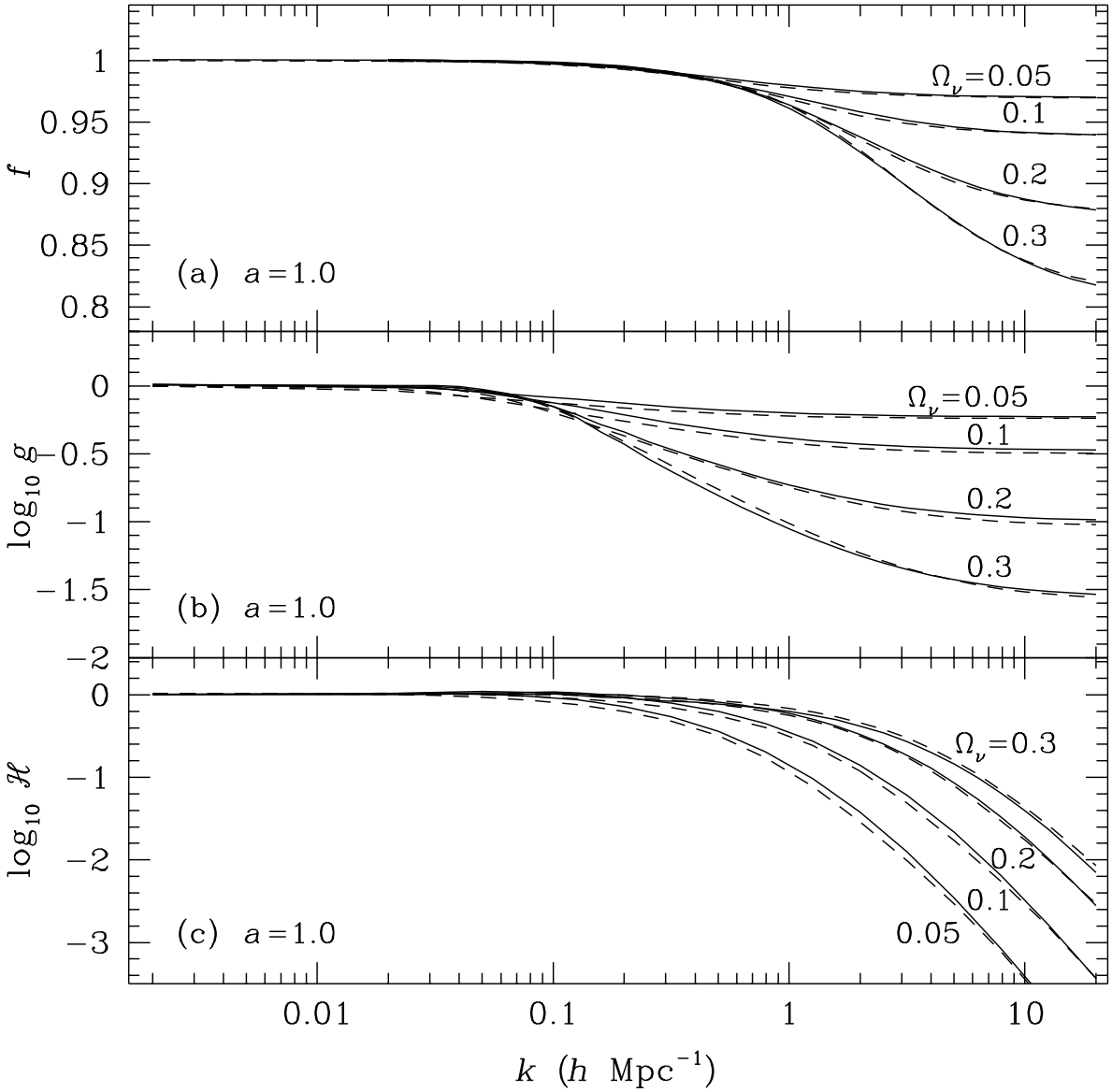

Fig. 2.— Direct integration of the Boltzmann equations (solid) vs. analytic fitting results (dashed) for the present-day CDM and HDM power spectra and the growth rate in four CDM+HDM models ($n = 1, H_0 = 50$) with $\Omega_\nu = 0.05, 0.1, 0.2$, and 0.3. (a) Growth rate $f(k, a, \Omega_\nu)$ of the density field. The fitting formula is given by eq. (6). (b) Ratio of the CDM power spectrum in CDM+HDM models to that in the pure CDM model, $g = P_c(\Omega_\nu)/P_c(\Omega_\nu = 0)$. The fitting formula is given by eq. (9). (c) Ratio of the HDM to CDM power spectrum, $\mathcal{H} = P_\nu(\Omega_\nu)/P_c(\Omega_\nu)$. The fitting formula is given by eq. (10).

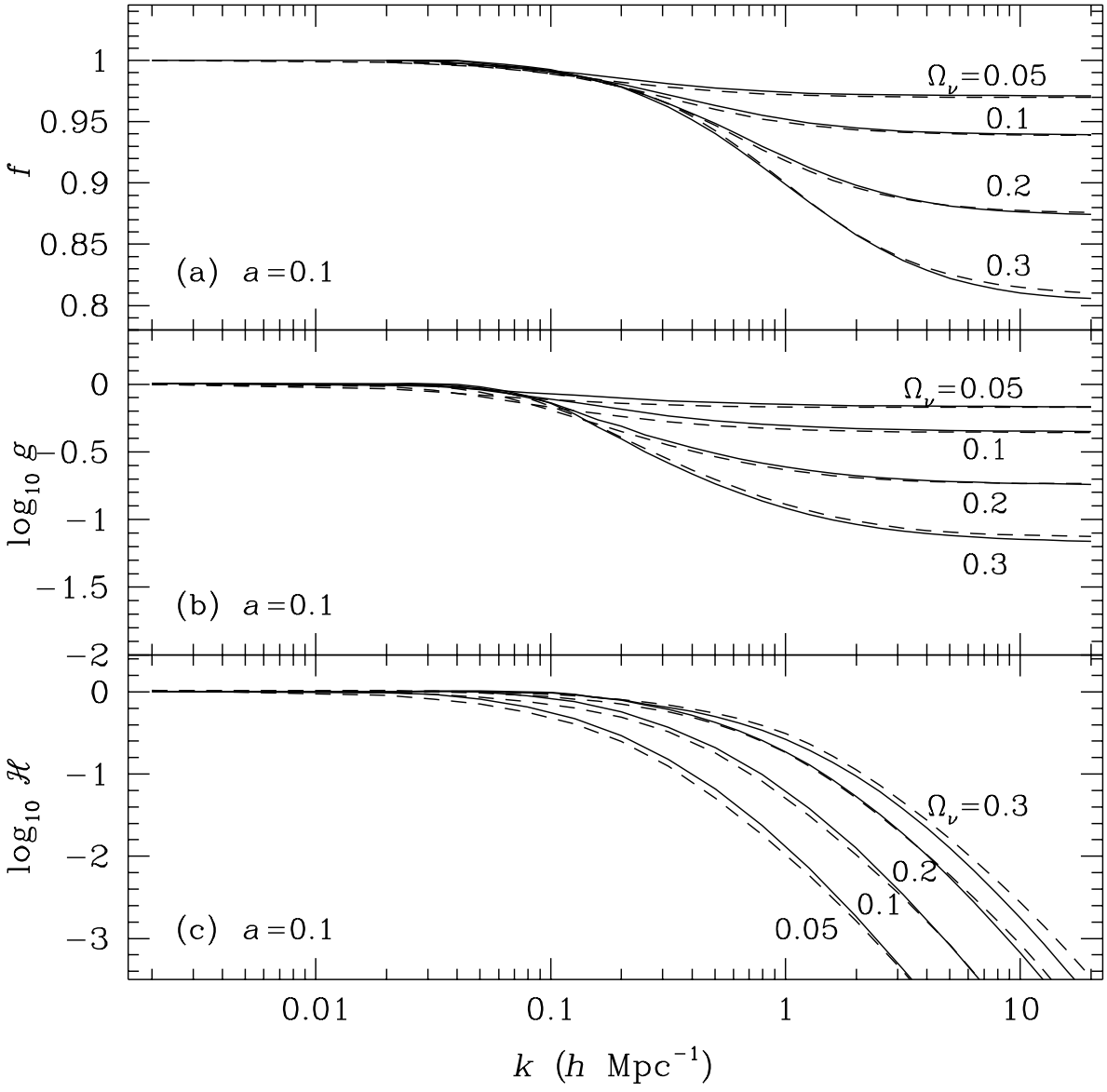

Fig. 3.— Same as Figure 2 but for $a = 0.1$

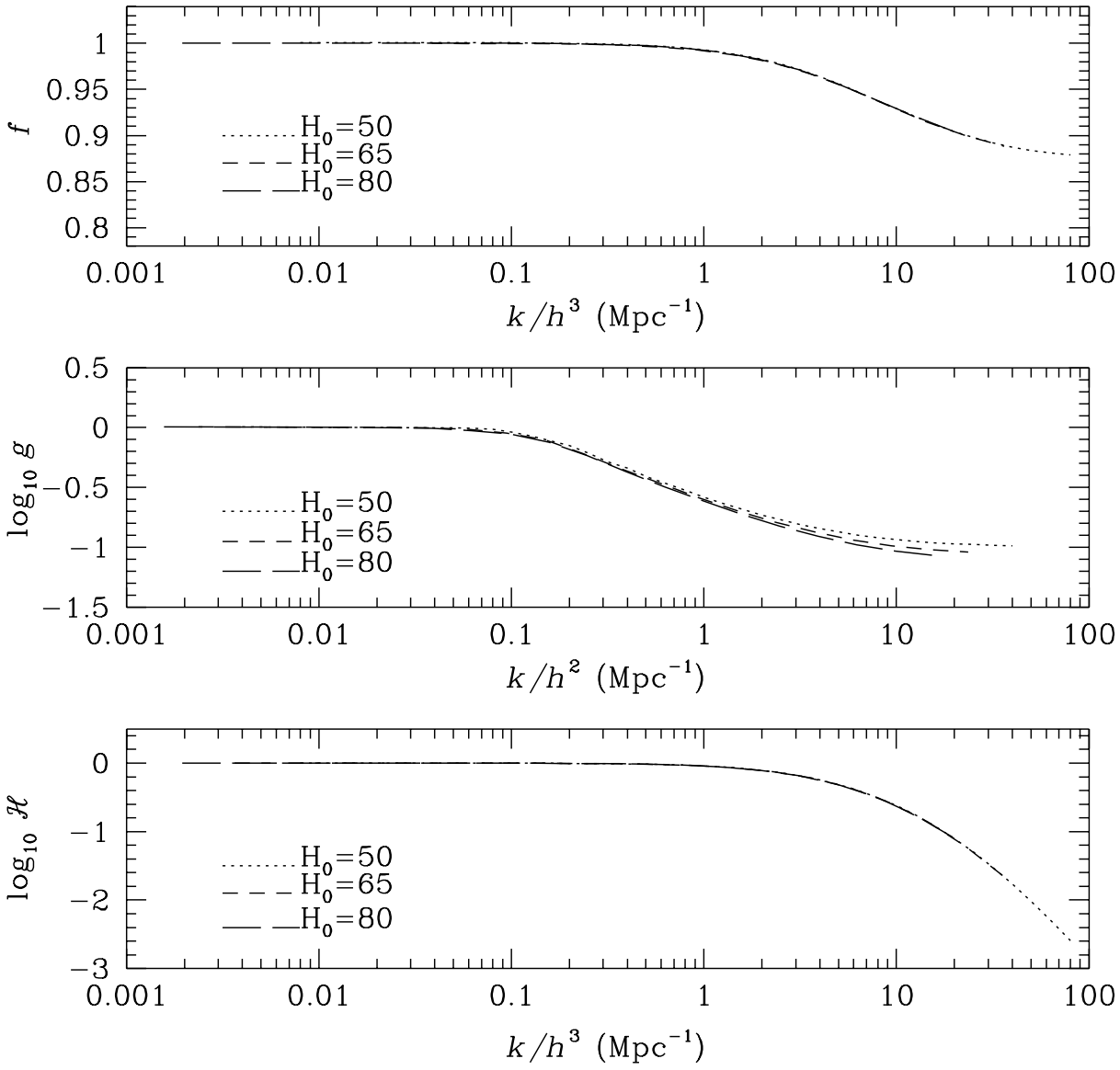

Fig. 4.— Scaling of k with the Hubble constant for functions f, g and $\mathcal{H}$ in the $\Omega_\nu = 0.2$, $n = 1$ CDM+HDM model at $a = 1$. As discussed in the text, f and $\mathcal{H}$ scale perfectly with k/h^3, while k/h^2 is a good approximation for g for a large range of k.

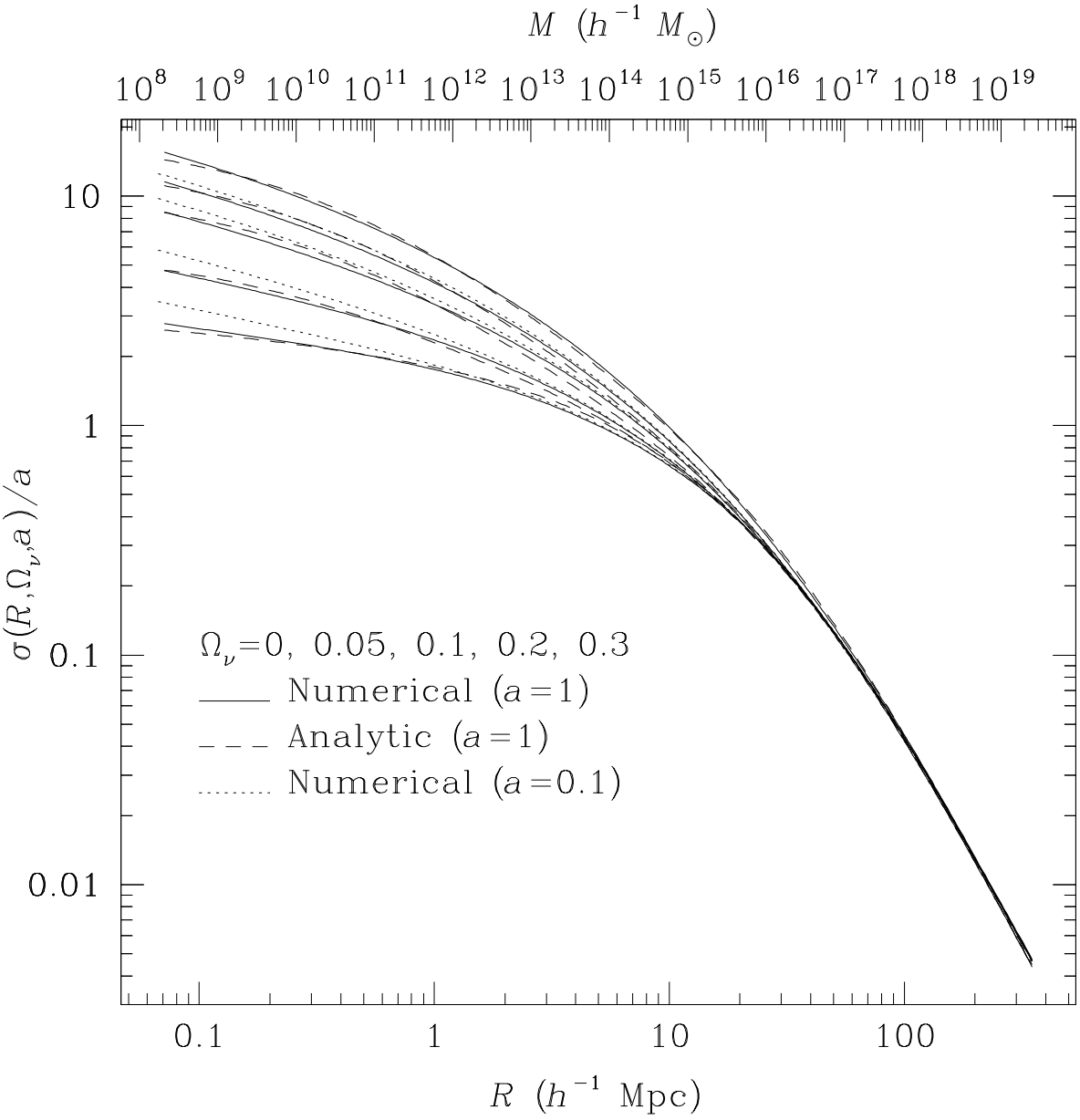

Fig. 5.— Root-mean-square of the linear mass fluctuations $\sigma(R, \Omega_\nu)$ in spheres of radius Rh^{-1} Mpc for $n = 1$ and $H_0 = 50$ models with $\Omega_\nu = 0.0, 0.05, 0.1, 0.2,$ and 0.3 (top down). The solid and dashed curves are from numerical integration and the fitting formulas eqs. (13) and (14), respectively. The dotted curves show the scaled $a^{-1}\sigma(R, \Omega_\nu\,, a)$ for $a = 0.1$, which start to deviate from $\sigma(R, \Omega_\nu, a = 1)$ only at small scale. All models are normalized to $Q_{\rm rms-PS} = 18\,\mu K$ at large R.

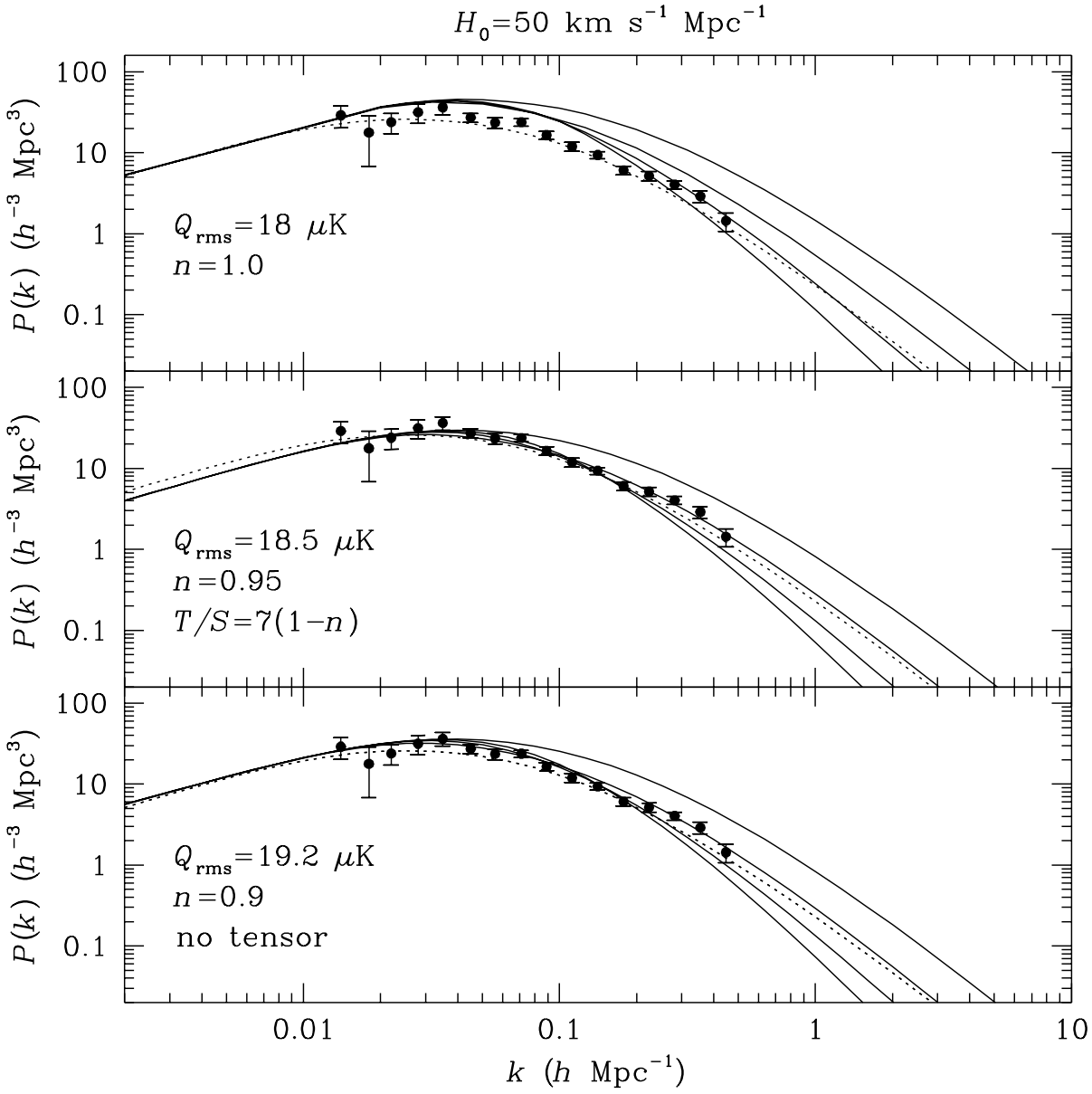

Fig. 6.— Density-weighted linear power spectrum for four models with neutrino fractions $\Omega_\nu = 0.0, 0.1, 0.2$ and 0.3 (solid curves from top down at large k), compared with the linear power spectrum reconstructed by Peacock & Dodds (1994) from galaxy and cluster surveys (filled symbols). The baryon fraction is $\Omega_b = 0.05$ and $H_0 = 50$ km s^{-1} Mpc^{-1}. The bottom two panels show the excellent agreement of CDM+HDM models with the data when the spectral index is reduced to $n = 0.95$ with tensor fluctuations (middle) or to $n = 0.9$ without tensor fluctuations (bottom). The 4-year COBE result is used for the normalization, and the dependence of $Q_{\rm rms-PS}$ on n is taken into account (see text). The dotted curves show an $n = 1$ CDM-type spectrum with a shape parameter of $\Gamma = \Omega h = 0.25$.

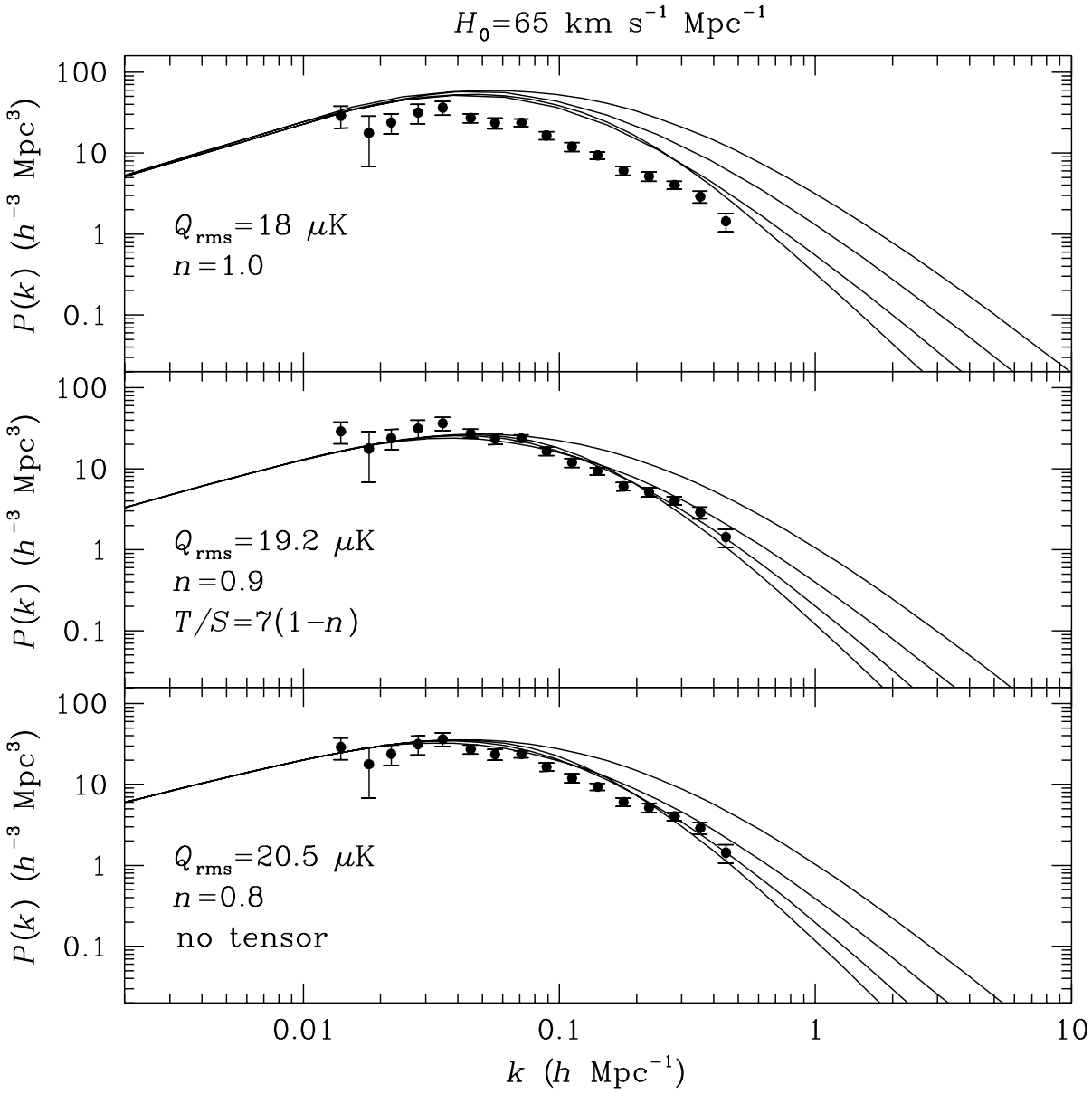

Fig. 7.— Same as Figure 6 but for $H_0 = 65$ km s^{-1} Mpc^{-1} (with $\Omega_b = 0.05$). A larger tilt of $n \approx 0.9$ (with tensor) or $n \approx 0.8$ (without tensor) is needed to reduce the excess power in the $n = 1$ model.

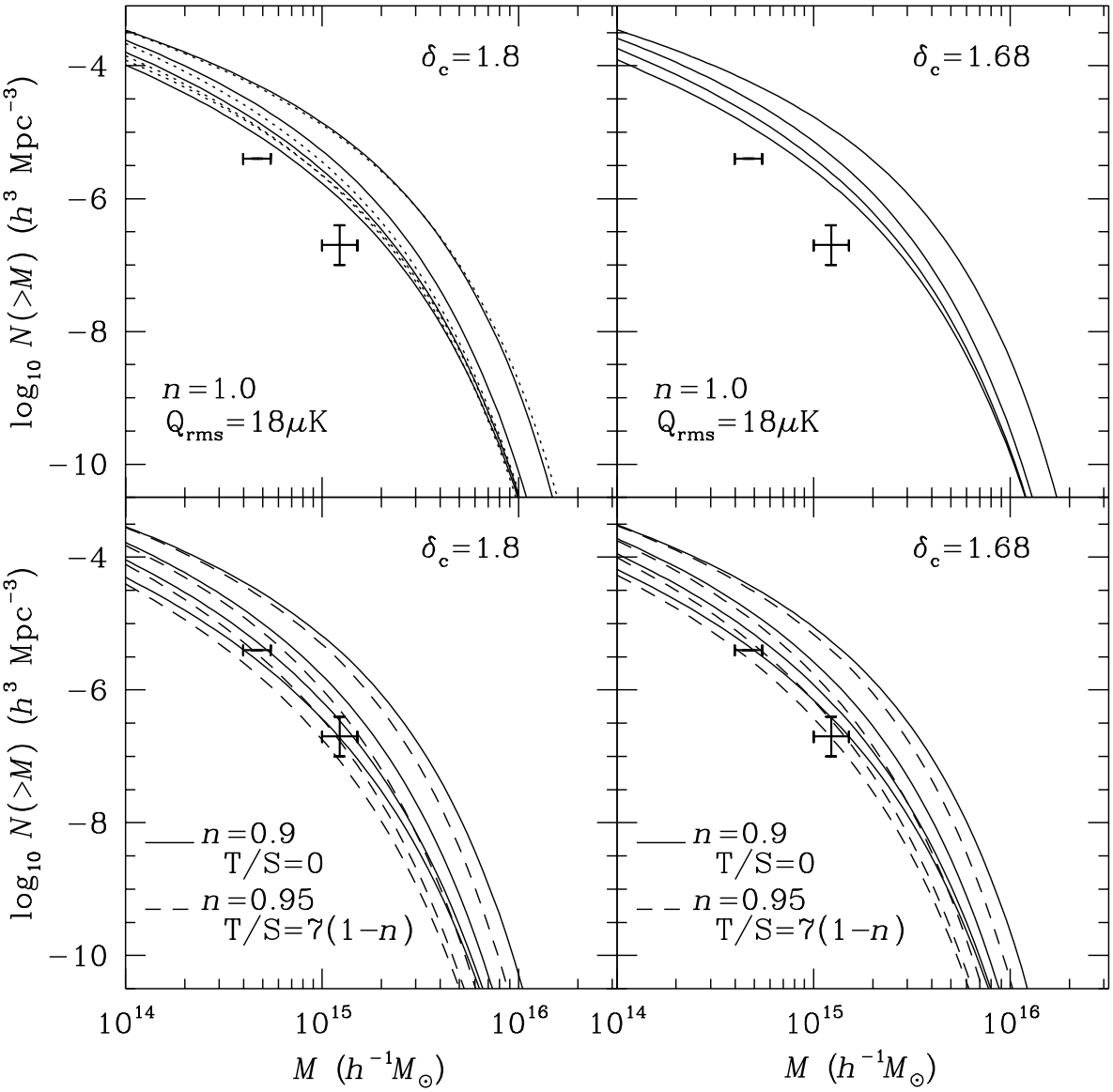

Fig. 8.— Present-day comoving number density of cluster-mass objects as a function of mass for the standard CDM and three CDM+HDM models. Different panels illustrate the effect of varying the spectral index n and the parameter δ_c in the Press-Schechter approximation. Top panels are for $n = 1$ models with $\Omega_\nu = 0$, 0.1, 0.2, and 0.3 (from top down), normalized to the 4-year COBE result $Q_{\rm rms-PS} = 18\,\mu K$ (Gorski et al. 1996). The solid and dotted curves in the upper left panel compare $N(> M)$ computed from numerical vs. fitted σ. Bottom panels show the same tilted models with $\Omega_\nu = 0$, 0.1, 0.2, and 0.3 (from top down) as in Figs. 6 and 7. The dependence of $Q_{\rm rms-PS}$ on n is taken into account: $Q_{\rm rms-PS} = 19.2\,\mu K$ for $n = 0.9$ and $Q_{\rm rms-PS} = 18.5\,\mu K$ for $n = 0.95$. The data points indicate the number density of clusters (Henry & Arnaud 1991) with X-ray temperature exceeding 3.7 (upper left) and 7 keV (lower right), respectively. The corresponding mass range is taken from White et al. (1993a) and Liddle et al. (1996).

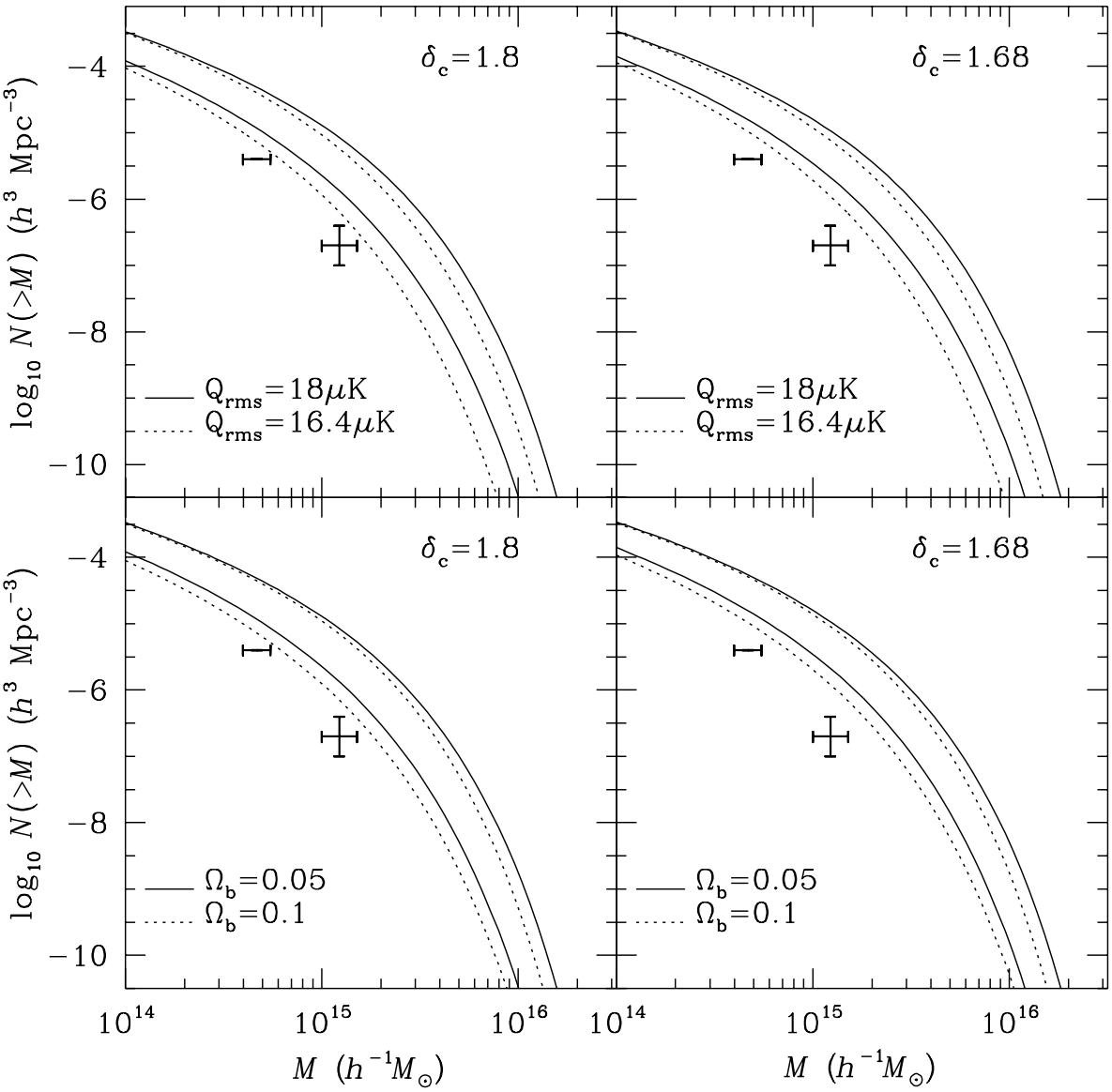

Fig. 9.— Effects of changing $Q_{\rm rms-PS}$ (upper panels) and Ω_b (lower panels) on the number density of cluster-mass objects. For clarity, only $\Omega_\nu = 0$ and 0.3 models are shown. All models have $n = 1$ and $h = 0.5$. The top panels assume $\Omega_b = 0.05$; the bottom panels assume $Q_{\rm rms-PS} = 18\,\mu K$. The data points are the same as in Fig. 8.